Monthly Notices of the ROYAL ASTRONOMICAL SOCIETY

MNRAS **493,** 807–814 (2020) doi:10.1093/mnras/staa322
Advance Access publication 2020 February 7

Mid-IR spectra of the M-type Mira variable R Tri observed with the *Spitzer* IRS

Dana K. Baylis-Aguirre,[1]★ M. J. Creech-Eakman[1] and Tina Güth[2]

[1]*Department of Physics, New Mexico Institute of Mining and Technology, 801 Leroy Place Socorro, NM 87801, USA*
[2]*Department of Astronomy, New Mexico State University, PO Box 30001, MSC 4500, Las Cruces, NM 88003, USA*

Accepted 2020 January 30. Received 2020 January 30; in original form 2019 October 8

ABSTRACT

We present analysis of mid-infrared (IR) spectra of the oxygen-rich Mira variable R Tri. The data were taken with the *Spitzer* Infrared Spectrometer (IRS) as part of a study tracking how Mira variables' regular pulsations affect circumstellar envelopes. We detected strong emission lines at 13.87, 16.18, and 17.6 μm, and one strong absorption feature at 14.98 μm. The emission features at 13.87 and 16.18 μm are excited vibrational bands of CO_2, while the absorption feature is the fundamental ν_2 band. The 17.6 μm emission feature has a completely different character than the molecular lines and we report its identification as Fe I fluorescence. We used a two-slab model with the radiative transfer code RADEX to model the CO_2 Q-branch bandheads. Our results indicate a slab of gas with T∼600 K located at ∼3–4 R_*. The cool temperature discrepancy with the radius provides observational evidence for the previously theoretical 'refrigeration zone'.

Key words: astrochemistry – line: formation – stars: AGB and post-AGB – stars: atmospheres – circumstellar matter – stars: late-type.

1 INTRODUCTION

1.1 Background and motivation

A fundamental topic in stellar physics is how stars create molecules and dust and return them back to the interstellar medium (ISM). Understanding this process affects many facets across astrophysics from star and planet formation to galaxy evolution. Molecules and dust contribute significantly to circumstellar environments, but our understanding of their creation is, at best, still rudimentary. We know a large fraction of material returned to the ISM is preferentially formed at the latest stages of stellar evolution [i.e. red giants, Asymptotic Giant Branch (AGB) stars, and supernovae], and that mass loss is a requisite activity throughout stellar evolution (Romano et al. 2010).

AGB stars are low-to-intermediate mass (0.8–8$M_\odot$) stars in the final stages of their evolution. They are characterized by hydrogen and helium shell burning on top of a degenerate carbon and oxygen core. Mira variables are AGB stars that pulsate regularly (periods of 100–500 d) with their visual amplitudes varying by up to several magnitudes. Miras variables have three chemical subclasses: oxygen-rich, C/O <1 (M-type), carbon-rich, C/O >1 (C-type), and intermediate, C/O ∼ 1 (S-type). The cool temperatures (2500–3500 K) of their photospheres allow for the creation of molecules and dust in the atmosphere and the pulsations help loft this material into the surrounding environment. These conditions make Mira atmospheres perfect laboratories for studying how evolved stars enrich the ISM.

Near and mid-infrared (mid-IR) spectroscopy provide the best opportunities for studying extended atmospheres surrounding Mira variables. Space-borne observations allow a study of wavelengths that are impossible to view with ground-based instruments due to telluric absorption. In the late 1990s and early 2000s, the *Infrared Space Observatory* (*ISO*, Kessler et al. 1996) made several crucial discoveries about molecules in Mira atmospheres. Yamamura et al. (1999a) reported the discovery of ro-vibrational band of SO_2 at 7.3 μm in three M-type Miras, which had previously only been observed in the millimetres (Lucas et al. 1986; Omont et al. 1993). T Cep had SO_2 bands that showed time variation moving from emission to absorption, but unfortunately the *ISO* observations only caught 1.4 periods and it was not determined if this was periodic behaviour or a transient event. Justtanont et al. (1998) and Ryde et al. (1998) independently reported the discovery of several ro-vibrational bands of CO_2 between 13 and 17 μm in several oxygen-rich AGB stars. The ν_2 fundamental band (bending mode) was sometimes observed in absorption while the excited bands were always seen in emission, but the variability could not be tied to the pulsation cycle. Justtanont et al. (1998) also noted that for AGB stars that exhibited the 13 μm dust feature the strength of this feature appeared to be correlated to the strength of the CO_2 emission features. Yamamura, de Jong & Cami (1999b) reported ro-vibrational bands of H_2O between 2.4 and 4 μm with variability that seemed to follow the pulsation cycle.

★ E-mail: dana.baylis@studemt.nmt.edu

These *ISO* observations clearly demonstrate that molecular layers surrounding Mira variables are dynamic, but more observations are required to understand what drives the observed variability.

The discovery of CO_2 in oxygen-rich sources is particularly interesting because until the *ISO* observations it was believed that the majority of the carbon was locked in CO molecules. Most contemporary models assumed thermal equilibrium in AGB and Mira atmospheres, and did not take into account how pulsation-driven shock waves could affect circumstellar chemistry. Duari, Cherchneff & Willacy (1999) suggested that the CO_2 forms in a region close to the photosphere of the star under non-equilibrium conditions created by shocks. To test this idea they created a model for the inner wind that experienced periodic shock waves from stellar pulsation and examined the chemistry in the cooling layers left behind in the post-shock region. The calculated abundances indicated that CO_2 was a product of shock chemistry after CO molecules were destroyed by OH radicals. Cherchneff (2006) used this wind model for the oxygen rich Mira TX Cam and reported consistent CO_2 abundances. The model also showed CO_2 is a good candidate for discriminating between M- and C-type Mira variables because CO_2 stops forming in regions > 1 R_* for C-types due to lack of OH molecules. The authors point out that time-resolved observations are needed to provide additional insight crucial to understanding how the periodic shocks affect the chemistry.

In this paper, we present analysis of mid-IR observations of the M-type Mira variable R Tri taken with the Spitzer Infrared Spectrometer (IRS, Houck et al. 2004). These observations are part of an observing campaign of 25 Mira variables designed to study phase-dependent behaviour in their circumstellar environment (Creech-Eakman et al. 2012). This study provides the first opportunity since *ISO* to investigate Mira atmospheres in a wavelength range not permissible for ground-based instruments, and it provides an opportunity to study time-dependent behaviour of spectral lines as suggested by previous studies (e.g. Yamamura 2003; Cherchneff 2006). For data reduction see Section 2.2.1, and for resulting spectra see Section 3. The *Spitzer* observations were done in conjunction with a decade long study of AGB stars using the Palomar Testbed Interferometer (PTI, Creech-Eakman & Thompson 2009). Combining results from these two observational studies provides us with an unprecedented detail of the molecule and dust forming region in R Tri's atmosphere.

2 OBSERVATIONAL DATA

2.1 R Tri

This paper focuses on the oxygen-rich Mira variable R Tri, which has a fairly short period of 266 d and ranges from spectral type M3.5 to M8 over the pulsation cycle. Originally classified as 'featureless' in the 8–21 μm region in the IRAS Low Resolution Spectrometer catalogue (Olnon et al. 1986) R Tri was later determined to have modest silicate and dust emission by Sloan & Price (1998) and classified as an 'SE3'. Benson et al. (1990) detected both H_2O and SiO masers, and Jura (1994) determined a mass-loss rate of 1.1×10^{-7} $M_\odot$ yr^{-1}. Using the results from the improved *Hipparcos* data reduction (van Leeuwen 2007), we estimate its distance at 294 pc.

2.2 *Spitzer* observations

The observations presented in this paper are part of a larger study done with the *Spitzer Space Telescope*'s IRS (Houck et al. 2004) to characterize circumstellar environments surrounding Mira variables (Creech-Eakman et al. 2012). The data were acquired during *Spitzer* GO program 50717 during 2008–2009; for data reduction see Section 2.2.1. This study provides an opportunity to address questions previously raised by *ISO* observations about the dynamics of Mira atmospheres in a wavelength regime that is inaccessible from the ground. The stars included in this study were chosen based on two conditions: (1) multiple observations were possible during *Spitzer* Cycle 5, and (2) the stars were bright enough to obtain high signal-to-noise spectra, but not so bright as to saturate the detector. This high stellar flux required defringing algorithms in the data reduction therefore each star in the sample has a dedicated background. A 'typical' period for a Mira variable is roughly one year so observations were made approximately every month for a sampling rate of ∼0.1 of a pulsation phase. In the case of R Tri two observations were obtained on 2008 September 07 and 2008 October 02, and resulted in two spectra at phases $\phi = 0.153$ and 0.222, respectively (see Fig. 1).

2.2.1 *Data reduction*

Each spectrum in our data set was reduced individually by hand. This data reduction process is fully described in Creech-Eakman et al. (2012). First, a sky-subtracted stellar spectral image was created by subtracting a dedicated background spectral image from the stellar spectral image. The *Spitzer* IDL package IRSCLEAN (https://irsa.ipac.caltech.edu/data/SPITZER/docs/dataanalysistools/tools/irsclean/) was used to remove rogue/bad pixels including bad pixels found by hand in each spectra in addition to those automatically flagged by the program. The 'Spitzer IRS Custom Extractor' (SPICE) (https://irsa.ipac.caltech.edu/data/SPITZER/docs/dataanalysistools/tools/spice/) tool was used to extract the stellar spectral orders from the spectral images by assuming an extraction of a point source. The SPICE package used calibration data from the observations which was specific to the orbits and our GO program, along with the bad pixel masks to extract and calibrate the flux from the IRS spectra. Because all of our stars were bright, fringes created internally from the spacecraft could have polluted the observations. To account for this possibility the *Spitzer* IRSFRINGE (https://irsa.ipac.caltech.edu/data/SPITZER/docs/dataanalysistools/tools/irsfringe/) tool was used to 'defringe' each spectrum. The individual spectral orders were sewn together into one complete high-resolution (R∼600) spectrum, combining individual nods of each module to create the final spectrum. Fig. 1 shows the resulting spectra for R Tri.

3 SPECTRA

3.1 Line identification

3.1.1 *Molecular features*

The spectra in Fig. 1 show two strong emission features at 13.87 and 16.18 μm, a strong absorption feature at 14.98 μm, and two weaker emission features at 13.49 and 16.78 μm. We have identified these features as unresolved ro-vibrational Q-branch bands of $^{12}CO_2$; the absorption feature at 14.98 μm is due to the fundamental ν_2 mode, while the emission lines are created by excited states (Herzberg 1945; Gordon et al. 2017). An energy level diagram for CO_2 including the observed transitions is given in Fig. 2. The continuum between Q-branches is dominated by a plethora of much weaker P and R transitions. Strong Q-branch lines of $^{12}CO_2$ were first observed in AGB stars with *ISO* by Justtanont et al. (1998) and Ryde et al. (1998).

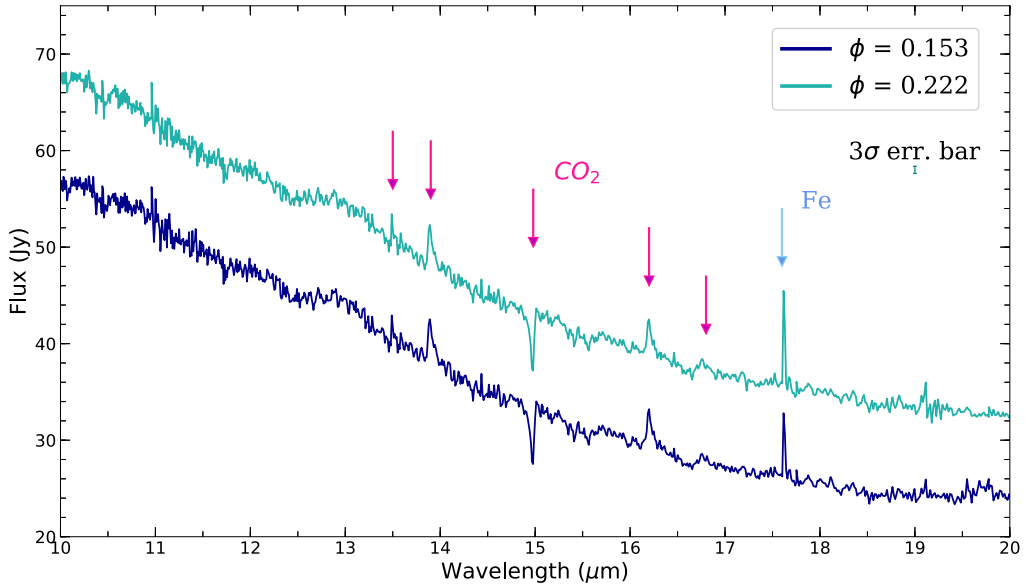

Figure 1. *Spitzer* IRS high-resolution (R ∼600) spectra of the M-type Mira variable R Tri. The top spectrum has been artificially offset upward 8 Jy for clarity.

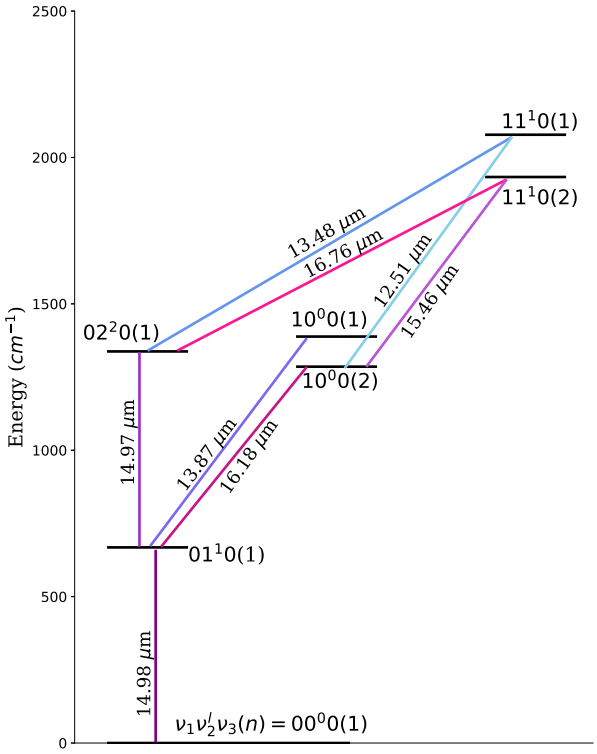

Figure 2. Vibrational energy diagram of CO_2 transitions included in RADEX model. The vibrational levels and Fermi split levels are labelled according to HITRAN's notation. The colours of the transitions match the bands calculated with RADEX that are shown in Fig. 3.

3.1.2 Atomic features

There is a bright emission feature centred at 17.6 μm seen in both phases and the narrowness of the line indicates that it is an atomic feature. We have consulted the Atomic Line List (van Hoof 2018) for identification and have preliminary identified this feature as Fe I fluorescence based on the available oscillator strengths and the strength of the emission. Fe fluorescence is commonly observed at other wavelengths in Mira atmospheres (Willson 1972; Luttermoser 1996, 2000). Further analysis of this feature will be presented in a later paper.

4 RADEX

We have chosen to model the CO_2 Q-branch bandheads using the radiative transfer code, RADEX (van der Tak et al. 2007) which is available as part of the Leiden Atomic and Molecular Database (LAMBDA, Schöier et al. 2005). We chose this this code for several reasons. First, it solves the radiative transfer using the Sobolev's approximation for expanding stellar envelopes (Sobolev 1960) an approach recommended strongly in Hubeny & Mihalas (2014) for stars with dynamic atmospheres such as Miras. Second, the code works under non-local thermodynamic equilibrium (NLTE) conditions, and this capability is vital because a priori we do not know if the CO_2 lines are formed under equilibrium conditions. Previous work done by Cherchneff (2006) and Duari et al. (1999) indicate the CO_2 gas must be created with dis-equilibrium conditions. Third, RADEX provides a step-up in model sophistication because it includes collisional affects where older models only required spectroscopic and dipole moment data for radiative transfer calculations. Most previous models fit lines separately, but RADEX calculates the radiative transfer for all lines included in the desired wavelength range. This allows us to fit multiple lines simultaneously which provides stronger constraints on the physical conditions creating the features. RADEX also provides flexibility by allowing the user to upload original molecular files for the calculations. We have created a custom molecular file for CO_2 that allows us to calculate the ro-vibrational transitions in Fig. 2 from 10 to 20 μm (for file details see Sections 4.1 and 4.2 below). A sample slab spectrum is presented in Fig. 3.

4.1 Molecular file

RADEX data files require detailed level energies, Einstein coefficients, and rate coefficients for collisional de-excitation for state-to-state transitions. There are data files of many molecules ready

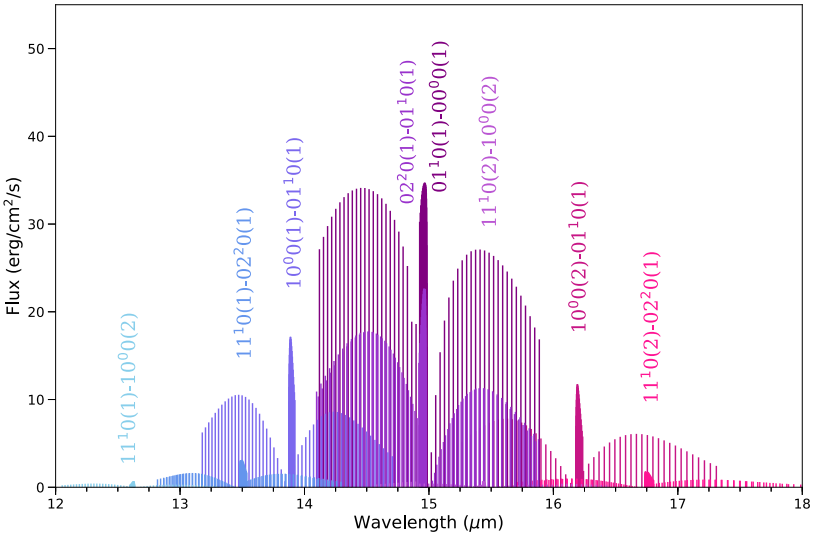

Figure 3. Sample slab spectrum of CO_2 calculated with RADEX. The colours of the bands match corresponding transitions shown in the energy level diagram in Fig. 2. Note the Q-branches build to the left or right according to the discussion in Section 5.1.

for modelling on the LAMBDA (Schöier et al. 2005), but most of these files are created for pure rotational transitions at longer wavelengths. We built a a custom data file for ro-vibrational transitions of CO_2 going up to $J = 50$, in the 10–20 μm range which includes over 700 radiative transitions and more than 18 000 collisional interactions with H_2 as the colliding partner. An energy level diagram of the CO_2 bands included in our file is presented in Fig. 2. Einstein A coefficients, and transition frequencies for CO_2 were taken from High-Resolution Transmission Molecular Absorption Database (HITRAN) (Gordon et al. 2017). Of the seven collision partners provided in the RADEX code (H_2, p-H_2, o-H_2, e^-, atomic H, He, and H^+) we have chosen H_2 as the colliding partner in all our calculations for two reasons: (1) H_2 is a dominant molecule in Mira atmospheres (Duari et al. 1999), and (2) most of the published laboratory data required to calculate the collisional rate coefficients were derived from experiments with H_2 collisions. Circumstellar environments surrounding Miras vary between several hundred and several thousand Kelvin. The collisional rate coefficients depend on temperature, thus, to account for the wide range of temperatures needed in Mira atmospheres we have used the results of CO_2 colliding with H_2 from Nevdakh, Orlov & Leshenyuk (2003) to extrapolate the temperature dependence of the $01^10\text{-}0^00$ vibrational rate for temperatures up to 1000 K. This temperature dependence was then applied to the remaining vibrational bands included in the file to create collisional rate coefficients for temperatures ranging from 100 to 1000 K in 50 K steps.

4.2 Collisional rate coefficients

As with Bosman, Bruderer & van Dishoeck (2017), we found no evidence of pure rotational transitions caused by CO_2 colliding with other species in the literature. To preserve ro-vibrational behaviour for our calculations we used ro-vibrational data of CO colliding with H_2 taken from Castro et al. (2017) which included transitions up to $J = 30$. For the remaining transitions, $J = 31$–50 were calculated using rotational data of CO colliding with H_2 taken from the LAMBDA data base. Rates for $J = 31$–40 were taken from Yang et al. (2010), while rates for $J = 41$–50 were taken from the high-J extrapolation file (Neufeld 2012). To calculate full state-to-state transitions, we followed methods similar to those presented in Bosman et al. (2017), Bruderer, Harsono & van Dishoeck (2015), Faure & Josselin (2008), and Chandra & Sharma (2001). Vibrational rates were combined with rotational rates to create full ro-vibrational rate coefficients. Rate coefficients between vibrational levels were taken from table A.1 in Bosman et al. (2017) or were calculated according to the relationship derived in Chandra & Sharma (2001) for $\nu > \nu'$:

$$k(\nu \rightarrow \nu') = \nu \frac{2\nu' + 1}{2\nu + 1} k(\nu = 1 \rightarrow \nu' = 0). \quad (1)$$

To calculate the full ro-vibration collisional rates from initial state ν, J to final state ν', J' we used the method suggested in Bosman et al. (2017) and Faure & Josselin (2008) to assume the vibrational levels can be decoupled from the rotational levels, that is, the rotational levels can be used to calculate a proportionality constant, $P_{J,J'}(T)$, that acts as a scaling factor on the vibrational rates:

$$k(\nu, J \rightarrow \nu', J') = P_{J,J'}(T) k(\nu \rightarrow \nu') \quad (2)$$

$$P_{J,J'}(T) = \frac{k(1, J \rightarrow 0, J') \Sigma_J g_J \exp(-E_{\nu,J}/kT)}{\Sigma_J (g_J \exp(-E_{\nu,J}/kT) \Sigma_{J'} k(1, J \rightarrow 0, J'; T))}. \quad (3)$$

Our proportionality equation differs slightly from the original expressions because we are not assuming the full rates are proportional to the rotational transitions inside the ground vibrational state as was done previously (e.g. Bosman et al. 2017; Bruderer et al. 2015). Instead, we assume the rates are proportional to rotational transitions from the $\nu = 1 \rightarrow \nu' = 0$ state in an effort to preserve as much ro-vibrational behaviour as possible for our model calculations. A sample slab spectrum calculated with RADEX is presented in Fig. 3 with model parameters: kinetic temperature = 750 K, H_2 density = 10^{12} cm^{-3}, CO_2 column density = 10^{16} cm^{-2}, background temperature = 300 K, and linewidth = 1 km s^{-1}. This spectrum reproduces consistent behaviour to the one calculated in Bosman et al. (2017) which uses similar parameters.

5 CO_2 MOLECULE

CO_2 is a fully symmetric linear molecule without a permanent dipole moment. It has four vibrational modes: a symmetric stretching mode (ν_1) at 1337 cm^{-1} , a doubly degenerate bending mode (ν_2) at 667 cm^{-1}, and an antisymmetric stretching mode (ν_3), at 2349 cm^{-1}. A vibrational state is then written as $\nu_1\nu_2^l\nu_3$, where l denotes angular momentum. The symmetric stretch is IR inactive because of CO_2's lack of a permanent dipole moment. Coincidentally, $\nu_1 \approx 2\nu_2$ and this accidental degeneracy allows for the eigenstates of $2\nu_2$ to perturb the eigenstates of ν_1, if they have identical angular momentum (Herzberg 1945). The vibrational states that have the same value of $2\nu_2 + \nu_1$ mix to the point that we can no longer unambiguously separate the individual levels. This mixing creates two vibrational levels that have slightly different energies in a phenomena called Fermi splitting. For example, the vibrational level $\nu_1\nu_2\nu_3 = 020$ has sub-levels 02^00 and 02^20 for $l = 0$ and 2, respectively. Only 02^00 can perturb and mix with the 10^00 level (both have $l = 0$) and vice versa , which creates two vibrational levels with distinct energies (Herzberg 1945). To account for Fermi splitting the vibrational state notation becomes $\nu_1\nu_2^l\nu_3(n)$; the Fermi levels created by the mixing of the 02^00 and the 10^00 states are then labelled as $10^00(1)$ and $10^00(2)$ following HITRAN's convention that ν_1 in Fermi split levels is determined by the state with the largest symmetric stretch quantum number. A vibrational level energy diagram for transitions included in our model is given in Fig. 2. The colours of the transitions match the corresponding bands shown in Fig. 3.

5.1 Ro-vibrational transitions

The structure of CO_2 emission is governed by transitions between the rotational ladders inside each vibrational level. Selection rules govern which transitions are permitted. Parallel bands obey $\Delta J = \pm 1$ and create P and R branches only. Perpendicular bands obey $\Delta J = 0$, $\Delta J = \pm 1$ creating a strong Q-branch in addition to the P and R branches. The P and R branches from adjacent bands overlap and blend together affecting the continuum. We are only modelling the macroscopic behaviour of the three strong CO_2 Q-branches at 13.87, 14.98, and 16.18 μm because we do not have the resolution to properly model all the nuances created with the P, R transitions blending together. The Q-lines build to the left or the right depending on whether the rotational constant is larger in the upper or the lower state (Ryde et al. 1998). Hence, the Q-transitions build to the left for the 14.98 μm line, but build to the right for the 13.87 and 16.18 μm lines. This trend is reflected in the slab spectrum produced using RADEX in Fig. 3.

6 MODEL

6.1 Slab model

We have chosen a slab model approach because although RADEX provides the expanding sphere as an option for the escape probability calculation this option does not include contributions from stellar winds or shocks. RADEX does provide a step up in sophistication from previous slab models for CO_2 which were not calculated in NLTE nor included collisions. We have adopted two slabs for modelling the CO_2 lines. The radiative transfer in each slab is calculated using RADEX and then the results are added to create a global fit all for all three features, rather than fitting each line individually. Ryde et al. (1998) suggest a multislab approach

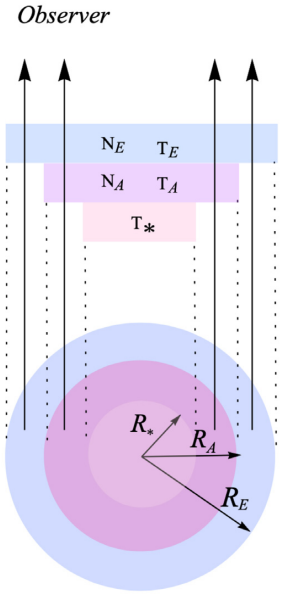

Figure 4. Conceptual two-layer slab model with an emitting layer sitting above an absorbing layer (not to scale). The layers are described by column density and kinetic temperature, which are calculated from RADEX models.

because the temperature structure needed to produce absorption at 14.98 μm in conjunction with satellite emission lines at 13.87 and 16.18 μm etc., requires a warm dense layer within several stellar radii in addition to an extended slightly cooler layer. Our model is focused on using the Q-branch bands to derive basic physical parameters for the CO_2 layers. We assume two adjacent uniform plane-parallel CO_2 layers superimposed on the stellar background source, as seen in Fig. 4. If the first slab is roughly the same size as the star it creates an absorbing layer (except when $T > T_*$), while the second layer is more extended and creates an emitting layer. The layers are described with two main parameters derived from the RADEX results, T_A and T_E; the kinetic temperatures of the absorbing and emitting layers, and N_A and N_E; the column densities of the absorbing and emitting layers. These are then used along with the optical depth calculated by RADEX to estimate the size of the slab of CO_2 gas as a function of R_*.

6.2 Stellar parameters

A simple blackbody did not fit the continuum well in the region of interest, most likely due to extra contribution from circumstellar dust species (Güth 2017). We therefore approximated the stellar background with a greybody continuum comprised of the sum of a blackbody function and a power law. The derived background temperatures for the first and second observations of R Tri are 2232 and 2462 K, respectively. The angular size of R Tri was determined to be 5.22 ± 0.30 mas using optical interferometric measurements taken with the PTI (Thompson, Creech-Eakman & Akeson 2002). Using this result with parallax data from *Hipparcos* (van Leeuwen 2007), we calculate the resulting stellar radius for R Tri to be 165 $R_\odot \pm 10\ R_\odot$.

6.3 RADEX parameters

RADEX requires several input parameters including, kinetic temperature, collision partner species, collision partner density, column

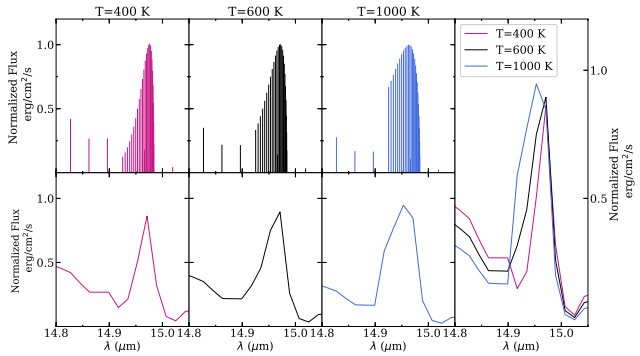

Figure 5. Temperature panel to demonstrate how temperature affects the behaviour of the 14.98 μm feature. Each calculation was done at the same column density, background temperature, and linewidth. Bands were calculated at 400, 600, and 1000 K. The bottom and right-hand side panels are the RADEX spectra smoothed to *Spitzer*'s IRS resolution. The temperature increase adds Q-branch transitions to the left causing the line centre to shift towards shorter wavelengths.

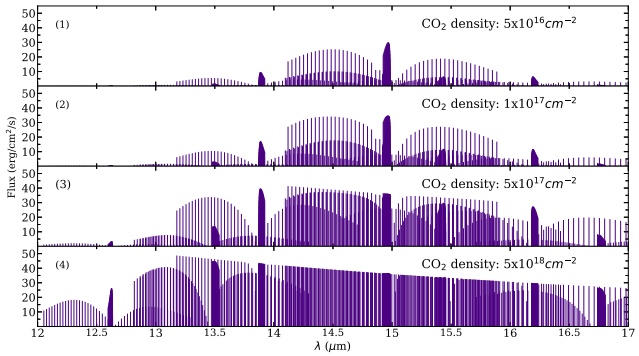

Figure 6. Density panel to demonstrate how the column density of CO_2 changes the intensity of the lines. All slab spectra were calculated at the same kinetic temperature, background temperature, and linewidth. Panel (1) was calculated at density 5×10^{16} cm^{-2}, panel (2) at 1×10^{17} cm^{-2}, panel (3) at 5×10^{17} cm^{-2}, and panel (4) at 5×10^{18} cm^{-2}. The optical depth increases with the density; the fundamental ν_2 band is the first line to become optically thick, this can be seen in panel (3). Eventually, the column density reaches a point where the whole spectrum flattens into a continuum as seen in panel (4).

density, background radiation temperature, and linewidth. We tested a range of H_2 densities from 10^{10} to 10^{12} cm^{-3} based on the density profile presented in Reid & Menten (1997). We found that a density of 10^{10} cm^{-3} did not adequately reproduce the ν_2 absorption feature. There was not a significant difference in the calculation results between using a density of 10^{11} and 10^{12} cm^{-3}, therefore we set the H_2 density at 10^{12} cm^{-3} for all calculations because this is the gas density reported in Reid & Menten (1997) near the molecular photosphere in AGB stars. The linewidth is assumed to be the same for all transitions included in the calculation and includes thermal and turbulent effects. We set the linewidth to 1 km s^{-1} for all calculations because the winds in Mira atmospheres are on the order of one to tens of km s^{-1} which will not create significant Doppler or turbulence broadening of the lines.

6.3.1 *Kinetic temperature*

The temperature of the CO_2 gas plays a vital role in determining line behaviour. As the temperature increases higher rotational levels within a band become more populated causing the Q-branches to effectively broaden. This temperature dependence will shift the line centre either right or left, depending on if additional Q-branch transitions build to the left or right (see Section 5.1). This can be seen in Fig. 5 for the fundamental ν_2 band at 14.98 μm. All lines were calculated with the same column density (10^{14} cm^{-2}), background temperature (100 K), H_2 density (10^{12} cm^{-3}), and linewidth (1 km s^{-1}). As the temperature increases additional Q-branch transitions broaden the line and shift the band centre towards shorter wavelengths. Using this behaviour allows us to constrain the temperature in fits from RADEX.

6.3.2 *Column density*

The CO_2 column density also greatly affects the model spectra. Fig. 6 demonstrates how increasing the column density affects the calculated spectra. All three spectra were calculated using the same kinetic temperature (750 K), background temperature (300 K), H_2 density (10^{12} cm^{-3}), and linewidth (1 km s^{-1}). As the column density increases from 5 to 500 $\times$ 10^{16} cm^{-2} the resulting spectra show excited bands beginning to contribute and increasing line

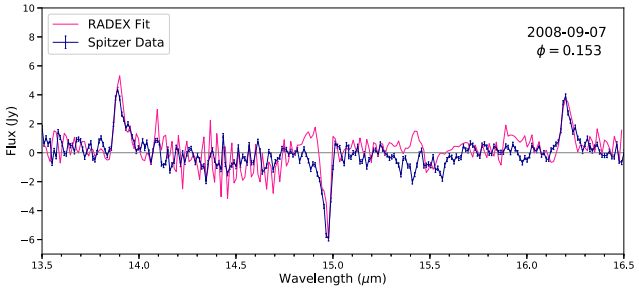

Figure 7. Result from two-layer slab model calculation performed with RADEX for R Tri 2008-09-07.

intensity. Increasing the column density also increases the optical depth and allows higher rotational levels to become populated. This causes line intensity to increase and the additional transitions also cause the lines to broaden. The first line to become optically thick is the fundamental ν_2 band at 14.98 μm (panel 3 in Fig. 6); increasing the column density past this point causes the spectrum to flatten into a continuum-like effect (panel 4 in Fig. 6).

7 RESULTS

The RADEX spectra calculated for the two R Tri observations are presented in Figs 7 and 8. The models targeted the ν_2 bending mode at 14.98 μm and the two excited bands at 13.87 and 16.18 μm. The strong absorption at 14.98 μm is not well reproduced from one single slab of CO_2; it requires contributions from both the absorbing layer close to the star and a surrounding emitting layer (see Fig. 4). The grid for the absorbing layer was built in 50 K steps in T_A and 0.05 $\times$ 10^{16} cm^{-2} steps in N_A, and the grid for the emitting layer had 50 K steps in T_E and 0.5 $\times$ 10^{17} cm^{-2} steps in N_E. These step sizes determine the uncertainties in temperature and column density. The step size for N_E is larger than N_A because the emission lines have greater optical depth and are thus higher up their respective curve of growth, making them less sensitive to changes in density. The fits were evaluated with eye-fitting and a χ^2 test. The slab model results and their uncertainties are presented

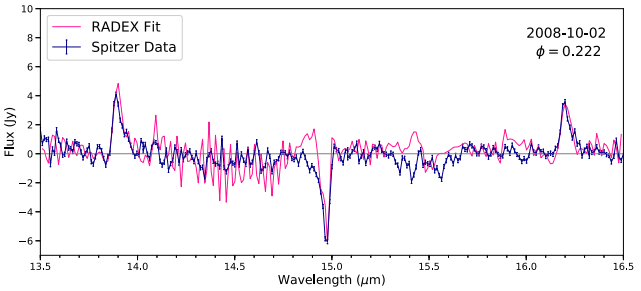

Figure 8. Result from two-layer slab model calculation performed with RADEX for R Tri 2008-10-02.

Table 1. RADEX slab spectrum model results for R Tri 2008-09-07. The two-layer slab model has a cooler, denser absorbing layer close to the star with a warmer less dense layer laying above it. The optical depth for the emitting contribution is taken as the average of the optical depths of the 13.87 and 16.18 μm bands.

RADEX results R Tri 2008-09-07				
λ(μm)	T_{kin} (K)	N (cm^{-2})	T_{exc}	τ
14.98	550 ± 50	$2.25 \times 10^{16} \pm 0.05 \times 10^{16}$	607^{+46}_{-49}	$0.850^{+0.04}_{-0.02}$
13.87	600 ± 50	$5.0 \times 10^{17} \pm 0.5 \times 10^{16}$	597^{+49}_{-50}	$1.91^{+0.19}_{-0.19}$
16.18	600 ± 50	$5.0 \times 10^{17} \pm 0.5 \times 10^{16}$	597^{+49}_{-50}	$1.87^{+0.19}_{-0.18}$

Table 2. RADEX slab spectrum model results for R Tri 2008-10-02. The results are almost identical to those presented in Table 1 because the star is nearly the same phase as the previous observation. The optical depth for the emitting contribution is taken as the average of the optical depths of the 13.87 and 16.18 μm bands.

RADEX results R Tri 2008-10-02				
λ(μm)	T_{kin} (K)	N (cm^{-2})	T_{exc}	τ
14.98	550 ± 50	$2.40 \times 10^{16} \pm 0.05 \times 10^{16}$	605^{+46}_{-49}	$0.911^{+0.02}_{-0.02}$
13.87	600 ± 50	$4.50 \times 10^{17} \pm 0.5 \times 10^{16}$	596^{+49}_{-50}	$1.72^{+0.19}_{-0.19}$
16.18	600 ± 50	$4.50 \times 10^{17} \pm 0.5 \times 10^{16}$	596^{+49}_{-50}	$1.69^{+0.18}_{-0.19}$

in Tables 1 and 2. The results are almost identical because the star is in almost the same pulsational phase in both observations. The absorbing layer has $T_{kin} = 550$ K, $N_A = 2.25$–2.4×10^{16} cm^{-2}, and $\tau \approx 0.9$, while the emitting layer has $T_{kin} = 600$ K, $N_E = 4.5$–5.0×10^{17} cm^{-2}, and $\tau \approx 1.8$. Using the the RADEX parameters from both layers combined with the stellar size, we estimate the radius of the of the slabs to be $R \sim 3$–$4R_*$.

8 DISCUSSION

The CO_2 Q-branch bandheads at 13.87, 14.98, and 16.18 μm seen in Figs 7 and 8 are well reproduced by the RADEX slab spectra. The regions between the Q-branches are dominated by P and R transitions blending together to create a forest of lines; it is impossible to distinguish individual P and R bands at *Spitzer*'s resolution and thus no attempt was made to reproduce their behaviour in this work. The two absorption features at 15.3 and 15.6 μm are likely due to transitions from additional excited bands not included in our RADEX file, while the feature at 15.4 μm could be the ν_2 bending mode for $^{13}CO_2$. Averaging the results from both sets of observations the column density for the absorbing layer is $N_A \sim 2 \times 10^{16}$ cm^{-2}, and the column density for the emitting layer is

Table 3. Results on CO_2 from previous studies conducted with *ISO*. Specific lines are denoted (E) for emission, and (A) for absorption. [1]Yamamura et al. (1999b), [2]Cami et al. (2000), [3]Markwick & Millar (2000).

Previous model results			
Target	T_{exc} (K)	N (cm^{-2})	R (R$_*$)
o Cet[1]			
4.3 μm (A)	800	2.0×10^{17}	2.3
Z Cas[1]			
4.3 μm (A)	800	1.5×10^{18}	1.7
EP Aqr[2]			
λ = 13.48 μm (E)	700	3.2×10^{18}	4.4
λ = 13.87 μm (E)	500	3.2×10^{18}	8.6
λ = 14.98 μm (E)	350	1.0×10^{19}	9
λ = 16.18 μm (E)	550	3.2×10^{18}	7.2
R Cas[3]			
13.48 and 13.87 μm (E)	1100	2.0×10^{16}	3.2
14.98 μm (A)	900	5.0×10^{16}	NA
IRC + 10011[3]			
14.98 μm (A)	650	3.0×10^{16}	7

an order of magnitude higher $N_E \sim 5 \times 10^{17}$ cm^{-2}. The layers have an average excitation temperature, $T_{ex} \sim 600$ K. These results are consistent with previous models of CO_2 in AGB stars and Mira variables presented in Table 3. Markwick & Millar (2000) results are of particular interest because their observations of R Cas showed the 14.98 μm feature in absorption with two excited emission bands at 13.5 and 13.87 μm and this was the only model of the three presented in Table 3 that attempted to fit multiple lines simultaneously rather than individually. The absorption feature could only be well fit if the model deviated from a thermal population of the 01^10 level and the authors argue that this deviation could be the result of collisional de-excitation with H_2, preferential formation of excited states, or an unknown pumping mechanism.

The location of the CO_2 gas at $R \sim 3$–4 R$_*$ is consistent with the molecule and dust formation zone in Mira atmospheres which typically lies 2–5 R$_*$ (e.g. Reid & Menten 1997; Wong et al. 2016). The temperature is several hundred Kelvin cooler than what we would expect at this radius, indicating a possible 'refrigeration' zone. Willson (2000) theorized a departure from radiative equilibrium which allows the temperature to drop in a region at several R$_*$, creating silicate dust closer to the star than previous models would allow, because silicate dust grains may require the temperature to be below 600 K for condensation (Gail & Sedlmayr 1998).

Recently, Wong et al. (2016) placed the inner dust formation radius at ∼4–5 R$_*$ for *o* Ceti. This is problematic for silicates which require lower temperatures to nucleate than this region would permit. Gail et al. (2013) argue that gas-phase SiO molecules nucleate into clusters and then condense on to grains and that SiO gas is depleted at temperatures ranging from 600 to 800 K (for mass-loss rates of 10^{-6}–10^{-4} M$_\odot$ respectively). Assuming the dust temperature is equivalent to the gas temperature at the inner boundary of the shell, this would allow silicate nucleation at closer distances than previously thought. However, models in Wong et al. (2016) showed that the SiO molecules will not deplete on to grains within ∼4 R$_*$. Güth (2017) used the DUSTY code to model dust species and abundances for M-type Miras and determined the spectra for R Tri showed the clear presence of calcium and magnesium silicates. Our results place a possible refrigeration zone

$\sim$3–4 R_* for R Tri and offers an alternative explanation for silicate nucleation within a few stellar radii. The plethora of CO_2 transitions accessible between 10 and 20 μm offer hundreds of possible radiative paths that could cool hot stellar photons escaping the photosphere and may contribute to the formation of this refrigeration zone.

9 CONCLUSION

Spitzer observations of the M-type Mira variable R Tri show several Q-branch band heads of CO_2 and a new bright emission feature at 17.6 μm. We built a molecular file of ro-vibrational transitions of CO_2 between 12 and 17 μm that can be used with RADEX to model CO_2 in the mid-IR. RADEX's capabilities of calculating the radiative transfer under NLTE conditions with collisional de-excitation with H_2 creates an advance in model sophistication. We used a two-slab RADEX model to simultaneously fit the three CO_2 Q-branches at 13.87, 14.98, and 16.18 μm. The model results indicate an extended layer of CO_2 gas located from $\sim$3–4 R_* with a kinetic temperature of $\sim$600 K. It is possible that this is observational evidence for a refrigeration zone which would permit silicate dust condensation within a few stellar radii. We will use RADEX to analyse the CO_2 lines in the remaining M-type Miras from the *Spitzer* study which will allow us to determine if the CO_2 gas undergoes any phase-dependent behaviour. We will use Echelon Cross-Echelle Spectrograph (EXES) on board SOFIA to observe a subset the M-type Miras included in the *Spitzer* study as part of SOFIA's Cycle 8 campaign. The higher resolution provided by EXES will allow us to put stronger constraints on the temperature and column density. SOFIA provides the first opportunity since *Spitzer* to observe CO_2 at these wavelengths, and the results from this work will provide an excellent starting point for future studies of CO_2 with SOFIA and JWST.

ACKNOWLEDGEMENTS

The authors wish to thank the referee for their comments and discussion. We also wish to thank A. Bosman for the private communication and discussion about collisional rate coefficients.This work is based [in part] on observations made with the Spitzer Space Telescope, which is operated by the Jet Propulsion Laboratory, California Institute of Technology under a contract with NASA. Support for this work was provided by NASA through an award issued by JPL/Caltech for Program GO 50717, under contract 1344355. This research has made use of NASA's Astrophysics Data System.

REFERENCES

Benson P. J., Little-Marenin I. R., Woods T. C., Attridge J. M., Blais K. A., Rudolph D. B., Rubiera M. E., Keefe H. L., 1990, ApJS, 74, 911
Bosman A. D., Bruderer S., van Dishoeck E. F., 2017, A&A, 601, A36
Bruderer S., Harsono D., van Dishoeck E. F., 2015, A&A, 575, A94
Cami J., Yamamura I., de Jong T., Tielens A. G. G. M., Justtanont K., Waters L. B. F. M., 2000, A&A, 360, 562
Castro C., Doan K., Klemka M., Forrey R. C., Yang B., Stancil P. C., Balakrishnan N., 2017, Mol. Astrophys., 6, 47
Chandra S., Sharma A. K., 2001, A&A, 376, 356
Cherchneff I., 2006, A&A, 456, 1001
Creech-Eakman M. J., Thompson R. R., 2009, in Luttermoser D. G., Smith B. J., Stencel R. E., eds, ASP Conf. Ser. Vol. 412, The Biggest, Baddest, Coolest Stars. Astron. Soc. Pac., San Francisco, p. 149
Creech-Eakman M. J., Güth T., Luttermoser D. G., Jurgenson C. A., Speck A. K., 2012, Astron. Rev., 7, 4
Duari D., Cherchneff I., Willacy K., 1999, A&A, 341, L47
Faure A., Josselin E., 2008, A&A, 492, 257
Gail H. P., Sedlmayr E., 1998, Faraday Discus., 109, 303
Gail H. P., Wetzel S., Pucci A., Tamanai A., 2013, A&A, 555, A119
Gordon I. E. et al., 2017, J. Quant. Spec. Radiat. Transf., 203, 3
Güth T., 2017, PhD thesis, New Mexico Institute of Mining and Technology
Herzberg G., 1945, in Herzberg G., ed., Molecular Spectra and Molecular Structure. Vol. 2, Infrared and Raman Spectra of Polyatomic Molecules, Van Nostrand, Reinhold, New York
Houck J. R. et al., 2004, in Mather J. C., ed., Proc. SPIE Conf. Ser. Vol. 5487, SPIE, Bellingham, p. 62
Hubeny I., Mihalas D., 2014, Theory of Stellar Atmospheres, Princeton Univ. Press, Princeton, NJ
Jura M., 1994, ApJ, 422, 102
Justtanont K., Feuchtgruber H., de Jong T., Cami J., Waters L. B. F. M., Yamamura I., Onaka T., 1998, A&A, 330, L17
Kessler M. F. et al., 1996, A&A, 500, 493
Lucas R., Omont A., Guilloteau S., Nguyen-Q-Rieu, 1986, A&A, 154, L12
Luttermoser D. G., 1996, in Pallavicini R., Dupree A. K., eds, ASP Conf. Ser. Vol 109, Cool Stars, Stellar Systems, and the Sun, Astron. Soc. Pac., San Francisco, p. 535
Luttermoser D. G., 2000, ApJ, 536, 923
Markwick A. J., Millar T. J., 2000, A&A, 359, 1162
Neufeld D. A., 2012, ApJ, 749, 125
Nevdakh V. V., Orlov L. N., Leshenyuk N. S., 2003, J. Appl. Spectrosc., 70, 276
Olnon F. M. et al., 1986, A&AS, 65, 607
Omont A., Lucas R., Morris M., Guilloteau S., 1993, A&A, 267, 490
Reid M. J., Menten K. M., 1997, ApJ, 476, 327
Romano D., Karakas A. I., Tosi M., Matteucci F., 2010, A&A, 522, A32
Ryde N., Eriksson K., Gustafsson B., Lindqvist M., Olofsson H., 1998, Ap&SS, 255, 301
Schöier F. L., van der Tak F. F. S., van Dishoeck E. F., Black J. H., 2005, A&A, 432, 369
Sloan G. C., Price S. D., 1998, ApJS, 119, 141
Sobolev V. V., 1960, Moving Envelopes of Stars, Harvard University Press, Cambridge
Thompson R. R., Creech-Eakman M. J., Akeson R. L., 2002, ApJ, 570, 373
van der Tak F. F. S., Black J. H., Schöier F. L., Jansen D. J., van Dishoeck E. F., 2007, A&A, 468, 627
van Hoof P. A. M., 2018, Galaxies, 6, 63
van Leeuwen F., 2007, A&A, 474, 653
Willson L. A., 1972, A&A, 17, 354
Willson L. A., 2000, ARA&A, 38, 573
Wong K. T., Kamiński T., Menten K. M., Wyrowski F., 2016, A&A, 590, A127
Yamamura I., 2003, in Nakada Y., Honma M., Seki M., eds, Astrophysics and Space Science Library, Vol. 283, Mass-Losing Pulsating Stars and their Circumstellar Matter. Springer-Verlag, Berlin, p. 173
Yamamura I., de Jong T., Onaka T., Cami J., Waters L. B. F. M., 1999a, A&A, 341, L9
Yamamura I., de Jong T., Cami J., 1999b, A&A, 348, L55
Yang B., Stancil P. C., Balakrishnan N., Forrey R. C., 2010, ApJ, 718, 1062

This paper has been typeset from a TEX/LATEX file prepared by the author.